Electronic Supplementary Material (ESI) for Dalton Transactions

Supporting Information for

Fluorescent single-ion magnets: molecular hybrid $(HNEt_3)[Dy_xYb_{1-x}(bpyda)_2]$ (x = 0.135−1)

Quan-Wen Li,[a,c] Jun-Liang Liu,[a,c] Jian-Hua Jia,*[a] Ji-Dong Leng,[a] Wei-Quan Lin,[a,b] Yan-Cong Chen,[a] and Ming-Liang Tong*[a,b]

[a] *MOE Key Lab of Bioinorganic and Synthetic Chemistry, State Key Laboratory of Optoelectronic Materials and Technologies, School of Chemistry & Chemical Engineering, Sun Yat-Sen University, Guangzhou 510275, P. R. China*

[b] *Lehn Institute of Functional Materials Sun Yat-Sen University, Guangzhou 510275, P. R. China*

[c] *These authors contributed equally to this work.*

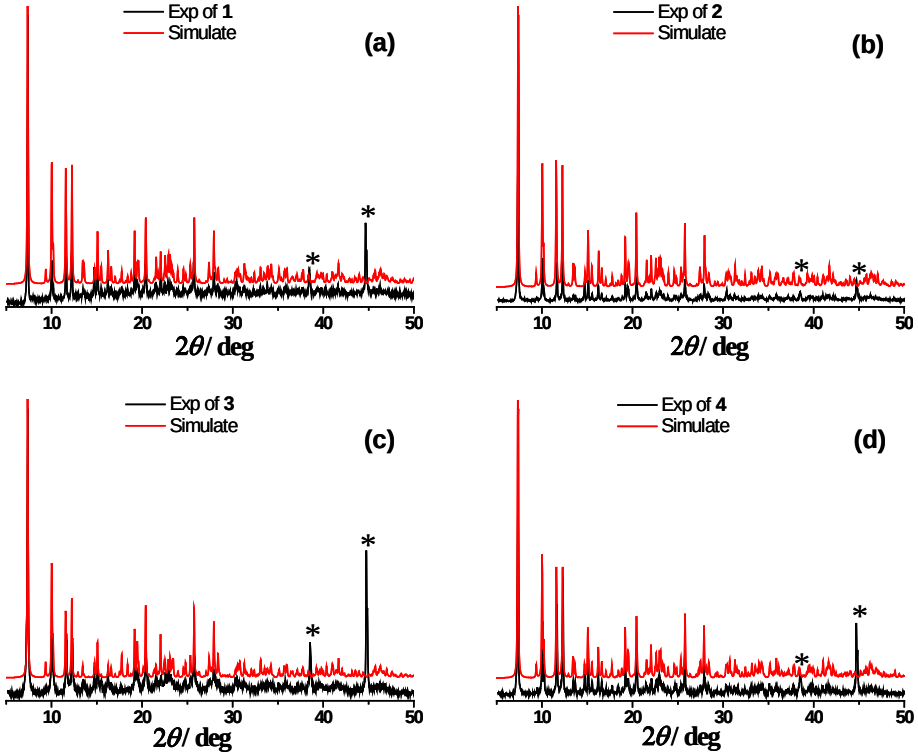

Figure S1. The experimental and simulated X-ray powder diffraction (XRPD) patterns of **1**-**4**. The peaks marked with * were due to silicon carrier.

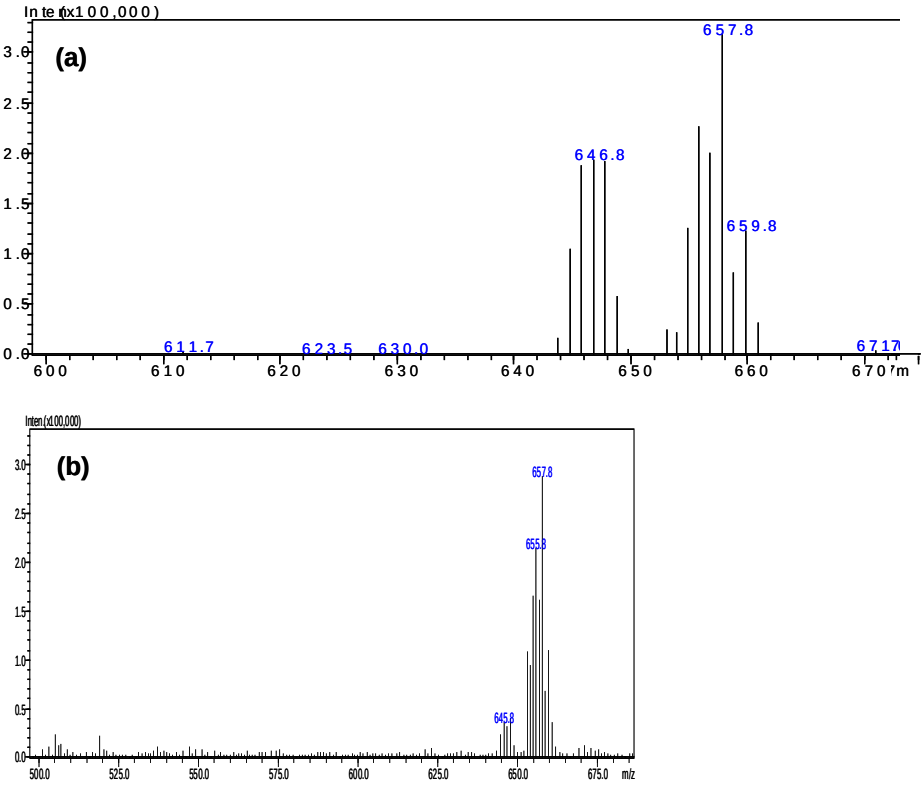

Figure S2. Single crystal MS show the ratio (Yb^{III} : Dy^{III}) of ca. 1.7 : 1 for **3** (**a**) and ca. 6.4 : 1 for **4** (**b**).

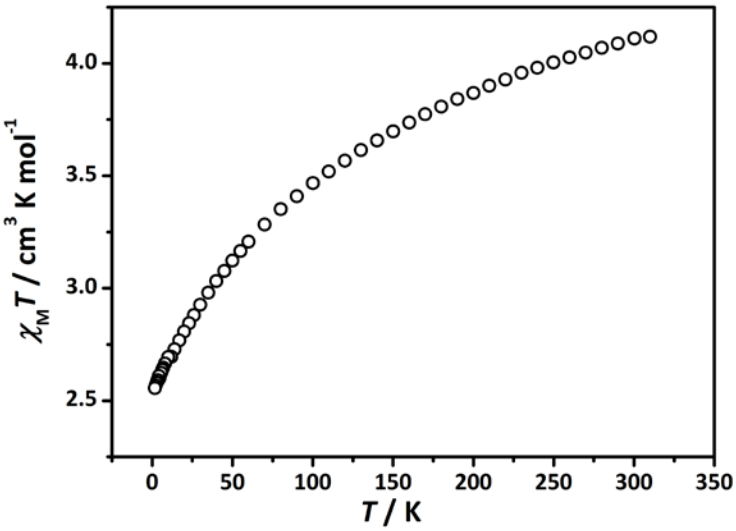

Figure S3. Temperature dependence of the $\chi_M T$ product of **4** at 500 Oe.

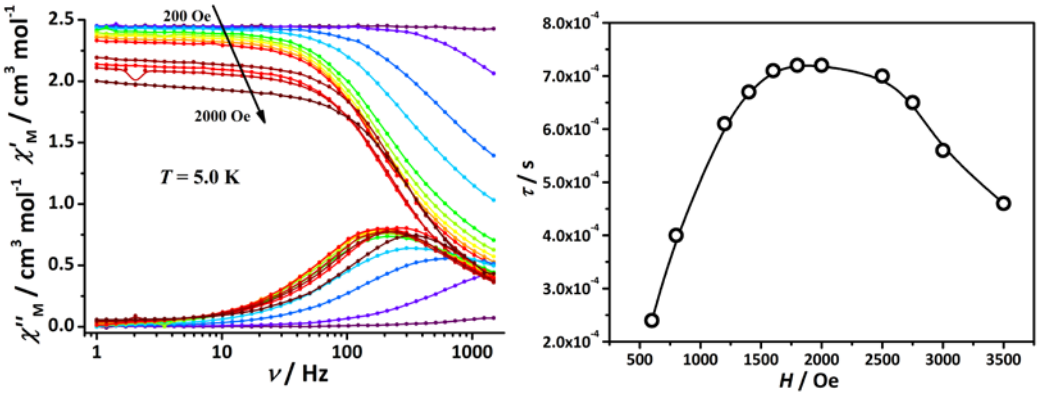

Figure S4. *Left*: Plot of ac susceptibility vs frequency oscillating at 1-1500 Hz at the indicated applied fields at 5.0 K for **1**. *Right*: dc field dependence of the relaxation time. The solid line is a guide for the eye.

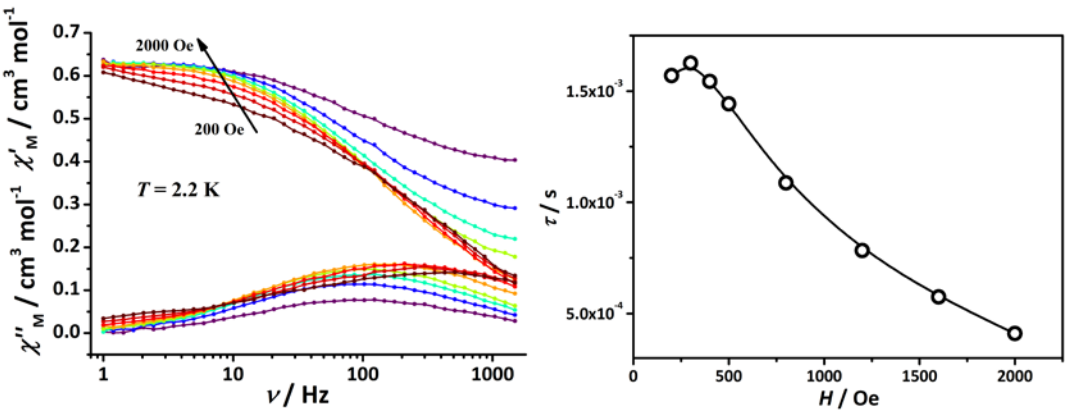

Figure S5. *Left*: Plot of ac susceptibility vs frequency oscillating at 1-1500 Hz at the indicated applied fields at 2.2 K for **2**. *Right*: dc field dependence of the relaxation time. The solid line is a guide for the eye.

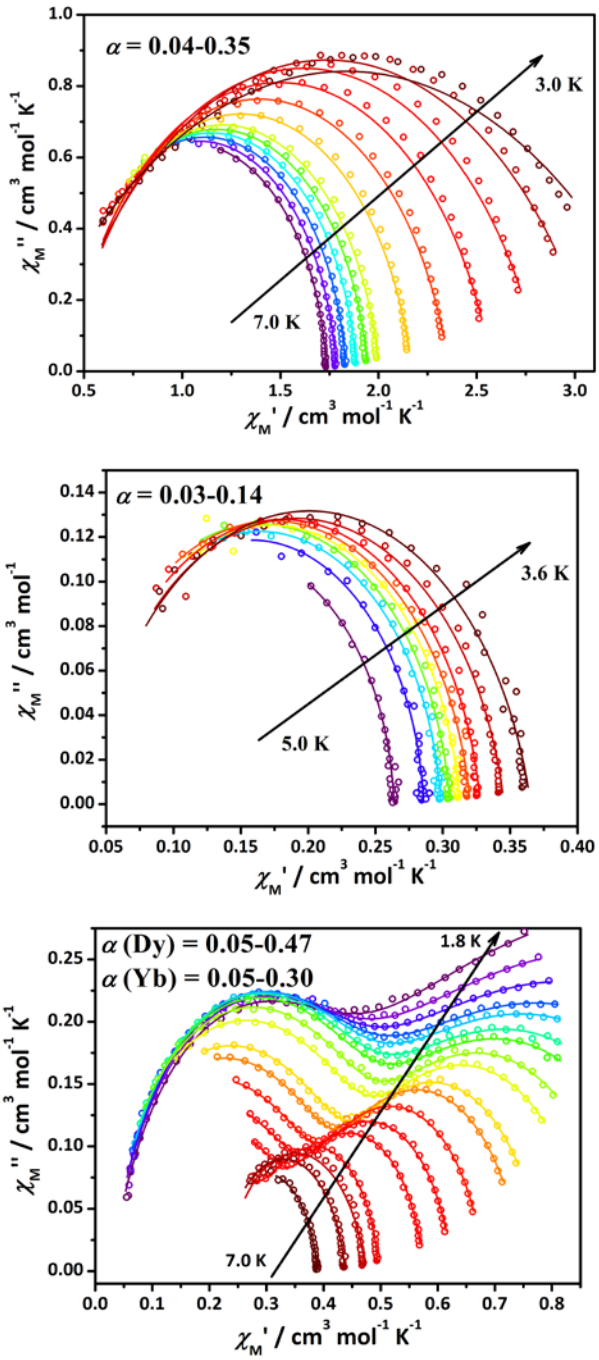

Figure S6. Cole-Cole plots for **1** (*left*), **2** (*middle*) and **4** (*right*) in the indicated temperature ranges. The solid lines represent the best fitting of the experimental data to a generalized Debye model for **1** and **2**, and a linear combination of two modified Debye functions for **4**.

For **1** and **2**: $$\chi_{ac} = \chi_S + \frac{(\chi_T - \chi_S)}{(1+i\omega\tau_1)^{1-\alpha}}$$

For **4**: $$\chi_{ac} = \chi_S + \frac{\Delta\chi_1}{(1+i\omega\tau_1)^{1-\alpha_1}} + \frac{\Delta\chi_2}{(1+i\omega\tau_2)^{1-\alpha_2}}$$

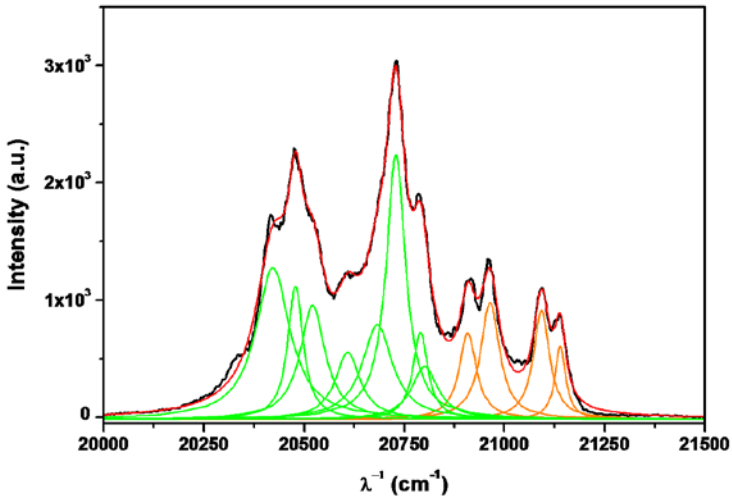

Figure S7. Simulation of the emission spectrum of the $^4F_{9/2}\rightarrow{}^6H_{15/2}$ transition of the microcrystalline **1** at 40 K through a convolution of Gaussian lines corresponding to the eight Kramers doublets (green lines) and four transitions arising from hot bands (orange lines).

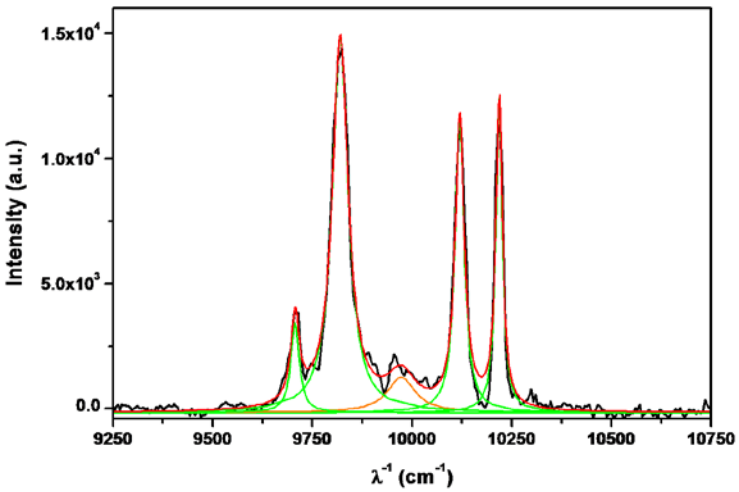

Figure S8. Simulation of the emission spectrum of the $^2F_{5/2}\rightarrow{}^2F_{7/2}$ transition of the microcrystalline **2** at 3 K through a convolution of Gaussian lines corresponding to the four Kramers doublets (green lines) and one transitions arising from hot bands (orange lines).

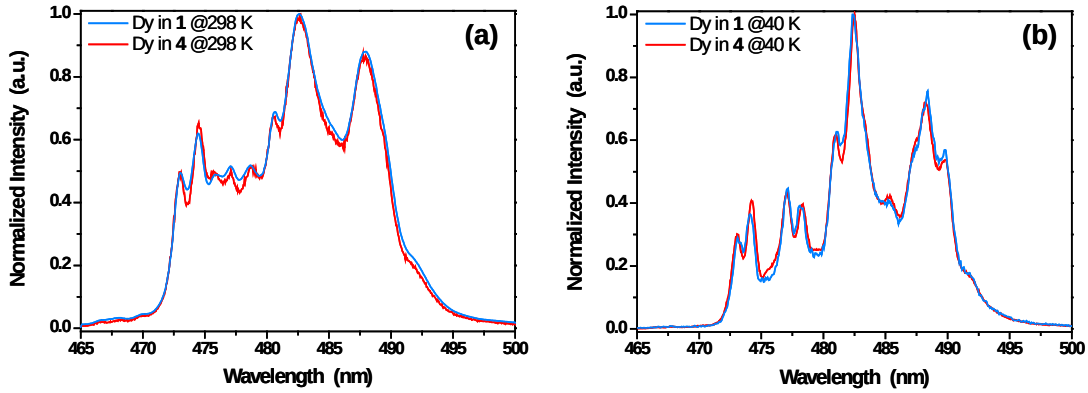

Figure S9. Emission spectra of the $^4F_{9/2}\rightarrow{}^6H_{15/2}$ transition of microcrystalline **1** and **4**.

Table S1. CShM values of the **1-4**.

Complex	Square Antiprism (D_{4d})	Triangular dodecahedron (D_{2d})	Biaugmented Trigonal Prism (C_{2v})
1	5.019	2.798	3.688
2	4.540	2.238	3.361
3	4.757	2.465	3.511
4	4.612	2.276	3.452

Table S2. Selected bond distances (Å) for **1-4**.

1		**2**		**3**		**4**	
Dy		Yb		$Dy_{0.367}Yb_{0.633}$		$Dy_{0.135}Yb_{0.865}$	
Dy−N	Dy−O	Yb−N	Yb−O	Ln−N	Ln−O	Ln−N	Ln−O
2.509(5)	2.350(4)	2.459(2)	2.298(2)	2.478(3)	2.321(3)	2.460(3)	2.302(2)
2.487(5)	2.311(4)	2.445(2)	2.285(3)	2.462(3)	2.300(3)	2.454(3)	2.289(3)
2.477(5)	2.311(4)	2.440(2)	2.274(2)	2.460(3)	2.294(3)	2.446(3)	2.282(3)
2.468(5)	2.305(5)	2.435(2)	2.259(2)	2.459(3)	2.286(3)	2.441(3)	2.263(2)
Average bond distances							
2.485	2.319	2.445	2.279	2.465	2.300	2.450	2.284

Table S3. Energy peak center (*Energy*, cm^{-1}) and full-width-at-half-maximum (*FWHM*, cm^{-1}) of the $^4F_{9/2}\rightarrow{}^6H_{15/2}$ Stark components of **1** calculating from simulation of the experimental emission spectrum excited at 332 nm at 40 K using multi-Gaussian function fit (R^2 = 0.99).

No.	1*	2*	3*	4*	5	6
Energy (cm^{-1})	21139.1	21092.1	20964.0	20908.2	20800.7	20790.0
FWHM (cm^{-1})	32.7	49.2	57.4	52.4	80.0	46.0
No.	7	8	9	10	11	12
Energy (cm^{-1})	20728.8	20682.5	20608.7	20521.2	20478.2	20421.7
FWHM (cm^{-1})	59.0	91.2	75.3	76.3	4.0	103.8

* "hot" bands arising from a thermally populated higher crystal-field sublevel of the $^4F_{9/2}$ state.

Table S4. Energy peak center (*Energy*, cm^{-1}) and full-width-at-half-maximum (*FWHM*, cm^{-1}) of the $^2F_{5/2}\rightarrow{}^2F_{7/2}$ Stark components of **2** calculating from simulation of the experimental emission spectrum excited at 338 nm at 3 K using multi-Gaussian function fit (R^2 = 0.98).

No.	1	2	3*	4	5
Energy (cm^{-1})	9706.5	9819.7	9973.1	10119.3	10218.1
FWHM (cm^{-1})	25.8	48.0	885.6	27.7	19.7

* "hot" bands arising from a thermally populated higher crystal-field sublevel of the $^2F_{5/2}$ state.

Table S5. Lifetime of microcrystalline **1**, **2**, **4** at room temperature.

Compound	**1**			**2**	**4**			
Ln ion	Dy			Yb	Dy			Yb
Wavelength (nm)	482	577	667	1011	482	577	667	1011
Lifetime (μs)*	29.60	29.34	29.28	6.58	17.34	18.16	18.00	13.99

* with error of ±0.03~0.14.